PERGAMON

International Journal of Solids and Structures 38 (2001) 7029–7044

INTERNATIONAL JOURNAL OF SOLIDS and STRUCTURES

www.elsevier.com/locate/ijsolstr

The self-thermal-plastic response of NiTi shape memory alloy fiber actuated metal matrix composites

William D. Armstrong [a,*], Torben Lorentzen [b,1]

[a] *Department of Mechanical Engineering, Thomas J. Watson School of Engineering and Applied Science, State University of New York at Binghamton, Binghamton, NY 13902-6000, USA*

[b] *Department of Materials Research, Risø National Laboratory, DK-4000 Roskilde, Denmark*

Received 14 January 1999; in revised form 1 December 2000

Abstract

The present work develops a quantitative theory of the self-thermal-plastic response of NiTi shape memory alloy actuated metal matrix composite materials. Model calculations are compared with existing experimental data obtained from a testing procedure consisting of an initial room temperature, 5% tensile elongation process, and a subsequent room temperature to 120°C unconstrained (external stress free) heating process. During the unconstrained heating process the composite fiber actuators attempt to recover pseudo-plastic strain imparted during the room temperature tensile prestrain process. As the temperature increases, the fiber stress–temperature state enters increasing phase transformation intensity, resulting in strong increases in fiber longitudinal tensile stress, matrix longitudinal compressive stress and composite compressive longitudinal external strain. Sufficient temperature brings the matrix stress state to the point of plastic yield. The composite then exhibits a very unusual, self-thermal-plastic compression response, recovering approximately 2.2% strain.

Keywords: Shape memory alloy fiber composite; Thermal elastic–plastic deformation; Phase transformation; Internal stress

1. Introduction

The technical utility of shape memory alloys stems from the ability of these materials to suffer reversible crystallographic transformations, and thereby recover large amounts of strain or exert large forces. The shape memory alloy material with the highest thermal–mechanical performance, and hence the highest applications potential is near equi-atomic NiTi. The basic crystallography of this material and basic thermal–mechanical behavior of these alloys has been studied both experimentally (Dautovich and Purdy, 1965; de Lange and Ziderveld, 1968; Knowles and Smith, 1981; Michal and Sinclair, 1981; Dunand et al., 1996; Jackson et al., 1972; Ling and Kaplow, 1980; Wayman, 1981; Otsuka and Shimizu, 1986; Miyazaki and Otsuka, 1986; Shaw and Kyriakides, 1995; Bo and Lagoudas, 1999) and theoretically (Tanaka and

* Corresponding author. Tel.: +1-607-777-6676; fax: +1-607-777-4620.

E-mail addresses: wda@binghamton.edu (W.D. Armstrong), torben.lorentzen@risoe.dk (T. Lorentzen).

[1] Tel.: +45-4677-5700; fax: +45-4677-5758.

0020-7683/01/$ - see front matter
PII: S0020-7683(00)00410-8

Nagaki, 1982; Liang and Rogers, 1990; Brinson, 1993; Brinson and Huang, 1996; Bo and Lagoudas, 1999) for many years.

Recently, attention has been focused on using NiTi shape memory alloys as fiber actuators within metal based smart composite materials (Wei et al., 1998). Early theoretical modeling efforts predicted the macroscopic thermal–mechanical behavior of various forms of such composites (Boyd and Lagoudas, 1994; Armstrong and Kino, 1995; Armstrong, 1996; Aboudi, 1997), while a set of pioneering experimental efforts explored processing methods and basic macroscopic thermal–mechanical behavior (Taya et al., 1993; Furuya et al., 1993; Armstrong and Kino, 1995; Hamada et al., 1998). Three experimental investigations proved in particular that an appropriately processed, room temperature prestrained NiTi shape memory fiber actuated aluminum metal matrix composite will exhibit large compressive strains during free heating. In the first of these, Armstrong and Kino (1995) subjected an experimental NiTi fiber 6061 aluminum alloy matrix composite to an initial room temperature prestrain treatment, a subsequent unconstrained heating process, and a final elevated temperature tensile process. The composite exhibited unusual hardening behavior during the prestrain process, a shape memory induced weak nonlinear thermal contraction during the unconstrained heating process, and a significantly increased flow strength at elevated temperature as compared to both the homogeneous matrix alloy and the room temperature composite. Armstrong and Lorentzen (1997), and later, Armstrong et al. (1998) significantly extended this work by investigating the room temperature prestrain followed by unconstrained heating behavior of a NiTi fiber 6082 aluminum matrix composite with in situ neutron diffraction. They further presented a one-dimensional thermal strain, internal stress and fiber phase transformation composite model, with parameters identified from extracted single fiber tests.

The present work extends beyond these earlier efforts to develop a quantitative theory of the self-thermal-plastic response of NiTi shape memory alloy actuated metal matrix composite materials. Model calculations are compared with recently obtained novel experimental data (Armstrong and Lorentzen, 2000). The present theory may be used by materials researchers for the analysis of experimental shape active metal matrix composite materials, and by mechanical engineers for the design of large deformation shape active structures and machine elements.

2. Modeling the multiaxial constitutive behavior of NiTi

2.1. NiTi transformation behavior

We begin our analysis by adopting an approach where austenite to martensite, or martensite to austenite phase transformation processes in NiTi are direct consequences of stress and temperature dependent transformation intensity distributions. Various simple stress–temperature paths may be imagined through a phase transformation domain connecting homogeneous end states. Transformation contours are defined as the locus of stress–temperature points at which particular partial phase contents first occur. An increment of nontrivial phase transformation may only occur during a forward stress–temperature displacement, a forward displacement being defined as one that penetrates a transformation contour for the first time in a given process. No phase transformation occurs if the stress–temperature state is displaced parallel to a transformation contour, or if the stress–temperature state suffers a reverse displacement.

We will restrict our attention to martensite to austenite phase recovery processes with forward variations in stress and temperature. By convention, we describe the phase content of NiTi by the martensite fraction, ξ. The martensite fraction is equal to 1 in a fully martensitic condition, and equal to 0 in a fully austenitic condition (Liang and Rogers, 1990).

Any change in martensite fraction is the sum of martensite fraction increments due to changes in temperature, $\mathrm{d}T$, and stress, $\mathrm{d}\bar{\sigma}^{\mathrm{f}}$.

$$\mathrm{d}\xi = \frac{\partial \xi}{\partial \bar{\sigma}^{\mathrm{f}}}\,\mathrm{d}\bar{\sigma}^{\mathrm{f}} + \frac{\partial \xi}{\partial T}\,\mathrm{d}T \tag{1}$$

The phase transformation increment due to a forward increment of stress during a M → A (martensite to austenite) shape recovery transformation is the product of the M → A transformation intensity with the pseudo-temperature increment $\mathrm{d}\bar{\sigma}^{\mathrm{f}}/C_{\mathrm{A}}$,

$$\frac{\partial \xi}{\partial \bar{\sigma}^{\mathrm{f}}}\,\mathrm{d}\bar{\sigma}^{\mathrm{f}} = \frac{\xi_0}{\sqrt{\pi}\sqrt{s_{\mathrm{a}}}} \exp\left[\frac{-\left(T - A_{\mathrm{a}} - \frac{\bar{\sigma}^{\mathrm{f}}}{C_{\mathrm{A}}}\right)^2}{s_{\mathrm{a}}}\right] \frac{\mathrm{d}\bar{\sigma}^{\mathrm{f}}}{C_{\mathrm{A}}} \tag{2}$$

where $\bar{\sigma}^{\mathrm{f}}$ is the fiber stress, T is the temperature, ξ_0 is the initial martensite fraction, C_{A} is the stress–temperature slope of the M → A mean transformation line, A_{a} is the M → A mean transformation line zero stress intercept, and s_{a} is the M → A distribution width parameter. Similarly, the martensite fraction increment due to a forward increment in temperature is the product of the martensite to austenite transformation intensity with the temperature increment $\mathrm{d}T$.

$$\frac{\partial \xi}{\partial T}\,\mathrm{d}T = -\frac{\xi_0}{\sqrt{\pi}\sqrt{s_{\mathrm{a}}}} \exp\left[\frac{-\left(T - A_{\mathrm{a}} - \frac{\bar{\sigma}^{\mathrm{f}}}{C_{\mathrm{A}}}\right)^2}{s_{\mathrm{a}}}\right] \mathrm{d}T \tag{3}$$

The total strain in the NiTi fiber is the sum of the fiber elastic mechanical, thermal and phase transformation strains,

$$\mathrm{d}\varepsilon^{\mathrm{f}} = \frac{\mathrm{d}\bar{\sigma}^{\mathrm{f}}}{E\{\xi\}} + \alpha_{\mathrm{f}}\,\mathrm{d}T + \varepsilon_{\mathrm{pl}}\,\mathrm{d}\xi \tag{4}$$

where $\varepsilon_{\mathrm{pl}}$ is the uniaxial strain recovered during a constant stress transformation from a completely stress induced martensite phase ($\xi = 1$) to a fully austenite phase ($\xi = 0$). Finally, we assume that the NiTi elastic modulus is linear in martensite fraction.

$$E\{\xi\} = E_{\mathrm{aus}} + \xi(E_{\mathrm{mar}} - E_{\mathrm{aus}}) \tag{5}$$

2.2. Generalization to multiaxial behavior

The one-dimensional incremental description of the shape memory alloy transformation behavior presented in the preceding section may be generalized to a multiaxial description by assuming a temperature and J_2 stress invariant dependent distributed transformation yield function,

$$\chi\left(T, J_2^{\mathrm{f}}\right), \quad J_2^{\mathrm{f}} = \tfrac{1}{2}\sigma_{ij}^{\mathrm{f}'}\sigma_{ij}^{\mathrm{f}'} \tag{6}$$

where $\sigma_{ij}^{\mathrm{f}'}$ is the fiber stress deviation. The fiber transformation intensities of Eqs. (2) and (3) will now be dependent on temperature and von Mises effective stress, $\bar{\sigma}^{\mathrm{f}} = (3J_2^{\mathrm{f}})^{1/2}$. Martensite to austenite transformation occurs when $\mathrm{d}\chi < 0$, neutral transformation occurs if $\mathrm{d}\chi = 0$, and elastic loading occurs if $\mathrm{d}\chi > 0$ in a way that is similar to conventional isotropic hardening plasticity. The transformation function associates a forward transformation intensity to every 10-dimensional stress–temperature coordinate. Fig. 1 shows a map of the martensite to austenite distributed transformation yield function in principle stress space. The object is four dimensional in principal stress space, expanding linearly with increases in temperature.

Mechanical stability requires that the incremental transformation strain tensor is at all times parallel to the transformation function divergence.

$$\mathrm{d}\varepsilon_{ij}^{\mathrm{ft}} = \mathrm{d}\lambda\,\frac{\partial \chi}{\partial \sigma_{ij}^{\mathrm{f}}} \tag{7}$$

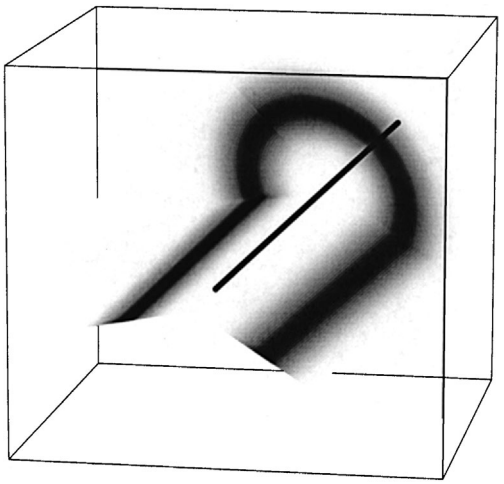

Fig. 1. Projection of the four-dimensional (one temperature and three principle stress coordinates) distributed martensite to austenite transformation intensity in stress space. The bold central line corresponds to a hydrostatic stress state. An increase in temperature results in the uniform radial expansion of the cylindrical transformation intensity distribution.

Eq. (8) may now be substituted into the von Mises effective strain relation,

$$\mathrm{d}\bar{\varepsilon}^{\mathrm{ft}} = \sqrt{\tfrac{2}{3}}\left(\mathrm{d}\varepsilon_{ij}^{\mathrm{ft}}\,\mathrm{d}\varepsilon_{ij}^{\mathrm{ft}}\right)^{1/2} \tag{8}$$

to identify $\mathrm{d}\lambda$.

$$\mathrm{d}\lambda = \sqrt{\tfrac{3}{2}}\frac{\mathrm{d}\bar{\varepsilon}^{\mathrm{ft}}}{\sqrt{\frac{\partial\chi}{\partial\sigma_{mn}^{\mathrm{f}}}\frac{\partial\chi}{\partial\sigma_{mn}^{\mathrm{f}}}}} \tag{9}$$

The multiaxial transformation strain is obtained by substituting the uniaxial transformation strain increment of the previous section,

$$\mathrm{d}\bar{\varepsilon}^{\mathrm{ft}} = \varepsilon_{\mathrm{pl}}\left(\frac{\partial\xi}{\partial\bar{\sigma}^{\mathrm{f}}}\,\mathrm{d}\bar{\sigma}^{\mathrm{f}} + \frac{\partial\xi}{\partial T}\,\mathrm{d}T\right) \tag{10}$$

into Eqs. (7) and (9).

$$\mathrm{d}\varepsilon_{ij}^{\mathrm{ft}} = \frac{\sqrt{\frac{3}{2}}\mathrm{d}\bar{\varepsilon}^{\mathrm{ft}}\,\frac{\partial\chi}{\partial\sigma_{ij}^{\mathrm{f}}}}{\sqrt{\frac{\partial\chi}{\partial\sigma_{mn}^{\mathrm{f}}}\frac{\partial\chi}{\partial\sigma_{mn}^{\mathrm{f}}}}} \tag{11}$$

3. Modeling the thermal–mechanical behavior of a NiTi fiber actuated metal matrix composite

We now use the results of the previous sections to predict the coupled internal stress, phase transformation and external strain behavior of a model shape memory alloy fiber reinforced elastic–plastic metal matrix composite. The complex nonlinear behavior of this material system requires an incremental approach.

3.1. Uniform stress model

The present study is directed at a composite with long, parallel fibers in the x_3 direction, we will use a modified permutation notation for the six independent components of the stress and strain tensors and their increments.

$$\sigma = [\sigma_{11},\ \sigma_{22},\ \sigma_{33},\ \sigma_{12},\ \sigma_{13},\ \sigma_{23}]^{\mathrm{T}} \tag{12}$$

$$\varepsilon = [\varepsilon_{11},\ \varepsilon_{22},\ \varepsilon_{33},\ 2\varepsilon_{12},\ 2\varepsilon_{13},\ 2\varepsilon_{23}]^{\mathrm{T}} \tag{13}$$

We will approximate the complicated local stress behavior of an actual composite by a simplified set of uniform stress relations (Dvorak and Bahei-El-Din, 1982). We first assume that the external average normal stress parallel to the fibers is given by the volume weighted sum of the individual fiber and matrix fiber parallel normal stresses,

$$\mathrm{d}\sigma_{33}^{\mathrm{ext}} = c_{\mathrm{f}}\,\mathrm{d}\sigma_{33}^{\mathrm{f}} + c_{\mathrm{m}}\,\mathrm{d}\sigma_{33}^{\mathrm{m}} \tag{14}$$

where the superscripts ext, f and m, as throughout this paper, denote external, fiber and matrix, c_{f} is the fiber volume fraction, c_{m} is the matrix volume fraction, and $c_{\mathrm{f}} + c_{\mathrm{m}} = 1$. All other stresses are assumed to be uniform between phases.

$$\mathrm{d}\sigma_{ij}^{\mathrm{ext}} = \mathrm{d}\sigma_{ij}^{\mathrm{f}} = \mathrm{d}\sigma_{ij}^{\mathrm{m}}, \quad ij \neq 33 \tag{15}$$

The individual phase stresses may be written as the product of a stress concentration tensor and the average external stress, these relations are equally applicable to elastic conditions or to conditions with fiber transformation and matrix plasticity.

$$\mathrm{d}\sigma^{\mathrm{f}} = B_{\mathrm{f}}\,\mathrm{d}\sigma^{\mathrm{ext}}, \qquad \mathrm{d}\sigma^{\mathrm{m}} = B_{\mathrm{m}}\,\mathrm{d}\sigma^{\mathrm{ext}} \tag{16}$$

By Eqs. (14) and (15), the stress concentration tensors obey a general volume equilibration,

$$c_{\mathrm{f}}B_{\mathrm{f}} + c_{\mathrm{m}}B_{\mathrm{m}} = I \tag{17}$$

where I is the identity matrix.

3.2. Elastic matrix behavior

Under purely elastic conditions the incremental stress in either the fiber or the matrix may be directly obtained from the incremental strain.

$$\mathrm{d}\sigma^{\mathrm{f}} = L_{\mathrm{fe}}\,\mathrm{d}\varepsilon^{\mathrm{f}}, \quad \mathrm{d}\sigma^{\mathrm{m}} = L_{\mathrm{me}}\,\mathrm{d}\varepsilon^{\mathrm{m}} \tag{18}$$

Inversion of the fiber and matrix elastic tensors allows the incremental strain to be directly obtained from the incremental stress,

$$\mathrm{d}\varepsilon^{\mathrm{f}} = M_{\mathrm{fe}}\,\mathrm{d}\sigma^{\mathrm{f}}, \qquad \mathrm{d}\varepsilon^{\mathrm{m}} = M_{\mathrm{me}}\,\mathrm{d}\sigma^{\mathrm{m}} \tag{19}$$

where

$$M_{\mathrm{fe}} = L_{\mathrm{fe}}^{-1} \quad \text{and} \quad M_{\mathrm{me}} = L_{\mathrm{me}}^{-1} \tag{20}$$

We now assume that the fiber and matrix total strains are the same in the fiber direction,

$$\mathrm{d}\varepsilon_{33}^{\mathrm{ext}} = \mathrm{d}\varepsilon_{33}^{\mathrm{fe}} + \mathrm{d}\varepsilon_{33}^{\mathrm{ft}} + \mathrm{d}T\alpha^{\mathrm{f}} = \mathrm{d}\varepsilon_{33}^{\mathrm{me}} + \mathrm{d}T\alpha^{\mathrm{m}} \tag{21}$$

where $\mathrm{d}T$ is the incremental temperature change, and α^{f}, α^{m} are the isotropic fiber and matrix coefficients of thermal expansion respectively, while all other external average strains are obtained as volume weighted sums of the individual phase strains.

$$\mathrm{d}\varepsilon_{ii}^{\mathrm{ext}} = c_{\mathrm{f}}\left(\mathrm{d}\varepsilon_{ii}^{\mathrm{fe}} + \mathrm{d}\varepsilon_{ii}^{\mathrm{ft}} + \alpha^{\mathrm{f}}\,\mathrm{d}T\right) + c_{\mathrm{m}}\left(\mathrm{d}\varepsilon_{ii}^{\mathrm{me}} + \alpha^{\mathrm{m}}\,\mathrm{d}T\right), \quad i = 1,2 \tag{22}$$

$$\mathrm{d}\varepsilon_{ij}^{\mathrm{ext}} = c_{\mathrm{f}}(\mathrm{d}\varepsilon_{ij}^{\mathrm{fe}} + \mathrm{d}\varepsilon_{ij}^{\mathrm{ft}}) + c_{\mathrm{m}}(\mathrm{d}\varepsilon_{ij}^{\mathrm{me}}), \quad ij = 12,13,23 \tag{23}$$

The fiber stress increment is then obtained from Eqs. (1)–(3), (6), (8), (11), (14)–(16), (18), and (21)–(23).

$$\left\{\mathrm{d}\sigma^{\mathrm{f}}\right\} = [B_{\mathrm{fe}}]\{\mathrm{d}\sigma^{\mathrm{ext}}\} + \left\{0,0,\frac{-\left(\mathrm{d}\varepsilon_{33}^{\mathrm{ft}} + \mathrm{d}T(\alpha^{\mathrm{f}} - \alpha^{\mathrm{m}})\right)}{M_{33}^{\mathrm{fe}} + \frac{c_{\mathrm{f}}}{c_{\mathrm{m}}}M_{33}^{\mathrm{me}}},0,0,0\right\}^{\mathrm{T}} \tag{24}$$

where B_{fe}, the fiber elastic stress concentration tensor, is written

$$B_{\mathrm{fe}} = \begin{bmatrix} 1 & 0 & 0 & 0 & 0 & 0 \\ 0 & 1 & 0 & 0 & 0 & 0 \\ B_{31}^{\mathrm{fe}} & B_{32}^{\mathrm{fe}} & B_{33}^{\mathrm{fe}} & B_{34}^{\mathrm{fe}} & B_{35}^{\mathrm{fe}} & B_{36}^{\mathrm{fe}} \\ 0 & 0 & 0 & 1 & 0 & 0 \\ 0 & 0 & 0 & 0 & 1 & 0 \\ 0 & 0 & 0 & 0 & 0 & 1 \end{bmatrix} \tag{25}$$

where

$$B_{31}^{\mathrm{fe}} = \frac{M_{31}^{\mathrm{fe}} - M_{31}^{\mathrm{me}}}{-M_{33}^{\mathrm{fe}} - \frac{c_{\mathrm{f}}}{c_{\mathrm{m}}}M_{33}^{\mathrm{me}}} \tag{26}$$

$$B_{32}^{\mathrm{fe}} = \frac{M_{32}^{\mathrm{fe}} - M_{32}^{\mathrm{me}}}{-M_{33}^{\mathrm{fe}} - \frac{c_{\mathrm{f}}}{c_{\mathrm{m}}}M_{33}^{\mathrm{me}}} \tag{27}$$

$$B_{33}^{\mathrm{fe}} = \frac{-\frac{1}{c_{\mathrm{m}}}M_{33}^{\mathrm{me}}}{-M_{33}^{\mathrm{fe}} - \frac{c_{\mathrm{f}}}{c_{\mathrm{m}}}M_{33}^{\mathrm{me}}} \tag{28}$$

$$B_{34}^{\mathrm{fe}} = \frac{M_{34}^{\mathrm{fe}} - M_{34}^{\mathrm{me}}}{-M_{33}^{\mathrm{fe}} - \frac{c_{\mathrm{f}}}{c_{\mathrm{m}}}M_{33}^{\mathrm{me}}} \tag{29}$$

$$B_{35}^{\mathrm{fe}} = \frac{M_{35}^{\mathrm{fe}} - M_{35}^{\mathrm{me}}}{-M_{33}^{\mathrm{fe}} - \frac{c_{\mathrm{f}}}{c_{\mathrm{m}}}M_{33}^{\mathrm{me}}} \tag{30}$$

$$B_{36}^{\mathrm{fe}} = \frac{M_{36}^{\mathrm{fe}} - M_{36}^{\mathrm{me}}}{-M_{33}^{\mathrm{fe}} - \frac{c_{\mathrm{f}}}{c_{\mathrm{m}}}M_{33}^{\mathrm{me}}} \tag{31}$$

The fiber stress increment is now written in terms of a typically unknown fiber effective stress increment and a typically known external applied stress and temperature increment. The correct fiber effective stress increment balances a first order Taylor expansion of the fiber stress increment.

$$\mathrm{d}\bar{\sigma}^{\mathrm{f}} = \frac{\partial\bar{\sigma}^{\mathrm{f}}}{\partial\sigma_{11}^{\mathrm{f}}}\,\mathrm{d}\sigma_{11}^{\mathrm{f}} + \frac{\partial\bar{\sigma}^{\mathrm{f}}}{\partial\sigma_{22}^{\mathrm{f}}}\,\mathrm{d}\sigma_{22}^{\mathrm{f}} + \frac{\partial\bar{\sigma}^{\mathrm{f}}}{\partial\sigma_{33}^{\mathrm{f}}}\,\mathrm{d}\sigma_{33}^{\mathrm{f}} + \frac{\partial\bar{\sigma}^{\mathrm{f}}}{\partial\sigma_{12}^{\mathrm{f}}}\,\mathrm{d}\sigma_{12}^{\mathrm{f}} + \frac{\partial\bar{\sigma}^{\mathrm{f}}}{\partial\sigma_{13}^{\mathrm{f}}}\,\mathrm{d}\sigma_{13}^{\mathrm{f}} + \frac{\partial\bar{\sigma}^{\mathrm{f}}}{\partial\sigma_{23}^{\mathrm{f}}}\mathrm{d}\sigma_{23}^{\mathrm{f}} \tag{32}$$

Once the fiber effective stress increment is known, the fiber stress increment is calculated from Eq. (24), and the matrix stress increment is given by

$$\{\mathrm{d}\sigma^{\mathrm{m}}\} = [B_{\mathrm{me}}]\{\mathrm{d}\sigma^{\mathrm{ext}}\} + \left\{0,0,\frac{\mathrm{d}\varepsilon_{33}^{\mathrm{ft}} + \mathrm{d}T(\alpha^{\mathrm{f}} - \alpha^{\mathrm{m}})}{\frac{c_{\mathrm{m}}}{c_{\mathrm{f}}}M_{33}^{\mathrm{fe}} + M_{33}^{\mathrm{me}}},0,0,0\right\}^{\mathrm{T}} \tag{33}$$

where B_{me}, the matrix elastic stress concentration tensor, is written

$$B_{\mathrm{me}} = \begin{bmatrix} 1 & 0 & 0 & 0 & 0 & 0 \\ 0 & 1 & 0 & 0 & 0 & 0 \\ B_{31}^{\mathrm{me}} & B_{32}^{\mathrm{me}} & B_{33}^{\mathrm{me}} & B_{34}^{\mathrm{me}} & B_{35}^{\mathrm{me}} & B_{36}^{\mathrm{me}} \\ 0 & 0 & 0 & 1 & 0 & 0 \\ 0 & 0 & 0 & 0 & 1 & 0 \\ 0 & 0 & 0 & 0 & 0 & 1 \end{bmatrix} \tag{34}$$

$$B_{31}^{\mathrm{me}} = \frac{M_{31}^{\mathrm{fe}} - M_{31}^{\mathrm{me}}}{\frac{c_{\mathrm{m}}}{c_{\mathrm{f}}}M_{33}^{\mathrm{fe}} + M_{33}^{\mathrm{me}}} \tag{35}$$

$$B_{32}^{\mathrm{me}} = \frac{M_{32}^{\mathrm{fe}} - M_{32}^{\mathrm{me}}}{\frac{c_{\mathrm{m}}}{c_{\mathrm{f}}}M_{33}^{\mathrm{fe}} + M_{33}^{\mathrm{me}}} \tag{36}$$

$$B_{33}^{\mathrm{me}} = \frac{\frac{1}{c_{\mathrm{f}}}M_{33}^{\mathrm{fe}}}{\frac{c_{\mathrm{m}}}{c_{\mathrm{f}}}M_{33}^{\mathrm{fe}} + M_{33}^{\mathrm{me}}} \tag{37}$$

$$B_{34}^{\mathrm{me}} = \frac{M_{34}^{\mathrm{fe}} - M_{34}^{\mathrm{me}}}{\frac{c_{\mathrm{m}}}{c_{\mathrm{f}}}M_{33}^{\mathrm{fe}} + M_{33}^{\mathrm{me}}} \tag{38}$$

$$B_{35}^{\mathrm{me}} = \frac{M_{35}^{\mathrm{fe}} - M_{35}^{\mathrm{me}}}{\frac{c_{\mathrm{m}}}{c_{\mathrm{f}}}M_{33}^{\mathrm{fe}} + M_{33}^{\mathrm{me}}} \tag{39}$$

$$B_{36}^{\mathrm{me}} = \frac{M_{36}^{\mathrm{fe}} - M_{36}^{\mathrm{me}}}{\frac{c_{\mathrm{m}}}{c_{\mathrm{f}}}M_{33}^{\mathrm{fe}} + M_{33}^{\mathrm{me}}} \tag{40}$$

The martensite fraction increment is obtained from Eqs. (1)–(3), and the external strain increment is given by Eqs. (22) and (23). The applied stress, temperature, fiber stress, fiber effective stress, matrix stress, fiber martensite fraction, fiber elastic modulus, and composite external strain are then updated in preparation for the solution of the next increment.

3.3. Plastic matrix behavior

We will assume that the initial yielding of the composite matrix is well described by a von Mises type yield function,

$$f = \tfrac{1}{2}\sigma_{ij}^{\mathrm{m}'}\sigma_{ij}^{\mathrm{m}'} - k^2 \tag{41}$$

where $\sigma_{ij}^{\mathrm{m}'}$ is the matrix stress deviation, matrix flow first occurs when $f = 0$, and k is equal to the yield stress under pure torsion. We make the further assumption that the matrix hardens kinematically in the manner proposed by Ziegler (1959). This means that each increment of plastic flow occurs on a yield function surface which is able to translate in stress space.

$$f(\sigma^{\mathrm{m}} - \psi) = 0 \tag{42}$$

The yield surface uniformly translates in the direction of the vector that joins the instantaneous center ψ with the matrix stress σ^{m}.

$$\mathrm{d}\psi = \mathrm{d}\mu(\sigma^{\mathrm{m}} - \psi) \tag{43}$$

the matrix stress state must remain on the yield surface after the loading increment.

$$\left\{\frac{\partial f}{\partial \sigma^{\mathrm{m}}}\right\}^{\mathrm{T}} (\mathrm{d}\sigma^{\mathrm{m}} - \mathrm{d}\psi) = 0 \tag{44}$$

$\mathrm{d}\mu$ may then be obtained by substitution of Eq. (43) into Eq. (44).

$$\mathrm{d}\mu = \left[\frac{\left\{\frac{\partial f}{\partial \sigma^{\mathrm{m}}}\right\}^{\mathrm{T}} \mathrm{d}\sigma^{\mathrm{m}}}{\left\{\frac{\partial f}{\partial \sigma^{\mathrm{m}}}\right\}^{\mathrm{T}} (\sigma^{\mathrm{m}} - \psi)}\right] \tag{45}$$

Mechanical stability requires that each increment of matrix plastic strain be orthogonal to the existing matrix yield surface.

$$\mathrm{d}\varepsilon_{ij}^{\mathrm{mp}} = \mathrm{d}\lambda \frac{\partial f}{\partial \sigma_{ij}^{\mathrm{m}}} \tag{46}$$

The matrix incremental plastic strain, $\mathrm{d}\varepsilon_{ij}^{\mathrm{mp}}$ is assumed to be proportional to the projection of $\mathrm{d}\sigma_{ij}^{\mathrm{m}}$ on the exterior normal of the yield surface (Ziegler, 1959).

$$\left(\mathrm{d}\sigma_{ij}^{\mathrm{m}} - c\,\mathrm{d}\varepsilon_{ij}^{\mathrm{mp}}\right)\frac{\partial f}{\partial \sigma_{ij}^{\mathrm{m}}} = 0 \tag{47}$$

Substituting Eq. (46) into Eq. (47) identifies $\mathrm{d}\lambda$,

$$\mathrm{d}\lambda_{\mathrm{m}} = \left[\frac{\left\{\frac{\partial f}{\partial \sigma^{\mathrm{m}}}\right\}^{\mathrm{T}} \mathrm{d}\sigma^{\mathrm{m}}}{c\left\{\frac{\partial f}{\partial \sigma^{\mathrm{m}}}\right\}^{\mathrm{T}} \left\{\frac{\partial f}{\partial \sigma^{\mathrm{m}}}\right\}}\right] \tag{48}$$

The flow parameter, c, may be referenced to experiment by the substitution of the plastic strain increment, obtained by the substitution of Eq. (48) into Eq. (46), into the matrix von Mises effective strain.

$$\mathrm{d}\bar{\varepsilon}^{\mathrm{mp}} = \sqrt{\tfrac{2}{3}}\left(\mathrm{d}\varepsilon_{ij}^{\mathrm{mp}}\,\mathrm{d}\varepsilon_{ij}^{\mathrm{mp}}\right)^{1/2} \tag{49}$$

The division of the von Mises incremental effective stress,

$$\mathrm{d}\bar{\sigma}^{\mathrm{m}} = \sqrt{\tfrac{3}{2}}\left(\mathrm{d}\sigma_{ij}^{m'}\,\mathrm{d}\sigma_{ij}^{m'}\right)^{1/2} \tag{50}$$

by the von Mises effective strain for processes in which the stress increment is parallel to the yield function normal identifies the constant c,

$$\frac{\mathrm{d}\bar{\sigma}^{\mathrm{m}}}{\mathrm{d}\bar{\varepsilon}^{\mathrm{mp}}} = \tfrac{3}{2}c = H_{\mathrm{m}} \tag{51}$$

as two-thirds the tangential modulus, H_{m}. The incremental matrix plastic strain may now be written as a direct function of existing stress state, stress increment and hardening parameter,

$$\{\mathrm{d}\varepsilon^{\mathrm{mp}}\} = \left(\frac{\left\{\frac{\partial f}{\partial \sigma^{\mathrm{m}}}\right\}^{\mathrm{T}} \{\mathrm{d}\sigma^{\mathrm{m}}\}}{\frac{3}{2H_{\mathrm{m}}}\left\{\frac{\partial f}{\partial \sigma^{\mathrm{m}}}\right\}^{\mathrm{T}} \left\{\frac{\partial f}{\partial \sigma^{\mathrm{m}}}\right\}}\right)\left\{\frac{\partial f}{\partial \sigma^{\mathrm{m}}}\right\} \tag{52}$$

The instantaneous matrix plastic compliance defined by

$$\{\mathrm{d}\varepsilon^{\mathrm{mp}}\} = [M^{\mathrm{mp}}]\{\mathrm{d}\sigma^{\mathrm{m}}\} \tag{53}$$

is obtained by the partial differentiation of the incremental matrix plastic strain.

$$M_{ij}^{\mathrm{mp}} = \frac{\partial \varepsilon_i^{\mathrm{mp}}}{\partial \sigma_j^{\mathrm{m}}} \tag{54}$$

We again require the fiber and matrix total strains to be identical in the fiber direction,

$$\mathrm{d}\varepsilon_{33}^{\mathrm{ext}} = \mathrm{d}\varepsilon_{33}^{\mathrm{fe}} + \mathrm{d}\varepsilon_{33}^{\mathrm{ft}} + \alpha^{\mathrm{f}}\,\mathrm{d}T = \mathrm{d}\varepsilon_{33}^{\mathrm{me}} + \mathrm{d}\varepsilon_{33}^{\mathrm{mp}} + \alpha^{\mathrm{m}}\,\mathrm{d}T \tag{55}$$

while all other external average strains are obtained as volume weighted sums of the individual phase strains.

$$\mathrm{d}\varepsilon_{ii}^{\mathrm{ext}} = c_{\mathrm{f}}(\mathrm{d}\varepsilon_{ii}^{\mathrm{fe}} + \mathrm{d}\varepsilon_{ii}^{\mathrm{ft}} + \alpha^{\mathrm{f}}\,\mathrm{d}T) + c_{\mathrm{m}}(\mathrm{d}\varepsilon_{ii}^{\mathrm{me}} + \mathrm{d}\varepsilon_{ii}^{\mathrm{mp}} + \alpha^{\mathrm{m}}\,\mathrm{d}T), \quad i = 1,2 \tag{56}$$

$$\mathrm{d}\varepsilon_{ij}^{\mathrm{ext}} = c_{\mathrm{f}}(\mathrm{d}\varepsilon_{ij}^{\mathrm{fe}} + \mathrm{d}\varepsilon_{ij}^{\mathrm{ft}}) + c_{\mathrm{m}}(\mathrm{d}\varepsilon_{ij}^{\mathrm{me}} + \mathrm{d}\varepsilon_{ij}^{\mathrm{mp}}), \quad ij = 12,13,23 \tag{57}$$

The fiber stress may then be identified using Eqs. (1)–(3), (6), (8), (11), (14)–(16), (49)–(53) and (55)–(57).

$$\left\{\mathrm{d}\sigma^{\mathrm{f}}\right\} = [B_{\mathrm{f}}]\{\mathrm{d}\sigma^{\mathrm{ext}}\} + \left\{0,0,\frac{-(\mathrm{d}\varepsilon_{33}^{\mathrm{ft}} + \mathrm{d}T(\alpha^{\mathrm{f}} - \alpha^{\mathrm{m}}))}{M_{33}^{\mathrm{fe}} + \frac{c_{\mathrm{f}}}{c_{\mathrm{m}}}(M_{33}^{\mathrm{me}} + M_{33}^{\mathrm{mp}})},0,0,0\right\}^{\mathrm{T}} \tag{58}$$

where B_{f}, the fiber stress concentration tensor, is written

$$B_{\mathrm{f}} = \begin{bmatrix} 1 & 0 & 0 & 0 & 0 & 0 \\ 0 & 1 & 0 & 0 & 0 & 0 \\ B_{31}^{\mathrm{f}} & B_{32}^{\mathrm{f}} & B_{33}^{\mathrm{f}} & B_{34}^{\mathrm{f}} & B_{35}^{\mathrm{f}} & B_{36}^{\mathrm{f}} \\ 0 & 0 & 0 & 1 & 0 & 0 \\ 0 & 0 & 0 & 0 & 1 & 0 \\ 0 & 0 & 0 & 0 & 0 & 1 \end{bmatrix} \tag{59}$$

where,

$$B_{31}^{\mathrm{f}} = \frac{M_{31}^{\mathrm{fe}} - M_{31}^{\mathrm{me}} - M_{31}^{\mathrm{mp}}}{-M_{33}^{\mathrm{fe}} - \frac{c_{\mathrm{f}}}{c_{\mathrm{m}}}(M_{33}^{\mathrm{me}} + M_{33}^{\mathrm{mp}})} \tag{60}$$

$$B_{32}^{\mathrm{f}} = \frac{M_{32}^{\mathrm{fe}} - M_{32}^{\mathrm{me}} - M_{32}^{\mathrm{mp}}}{-M_{33}^{\mathrm{fe}} - \frac{c_{\mathrm{f}}}{c_{\mathrm{m}}}(M_{33}^{\mathrm{me}} + M_{33}^{\mathrm{mp}})} \tag{61}$$

$$B_{33}^{\mathrm{f}} = \frac{-\frac{1}{c_{\mathrm{m}}}\left(M_{33}^{\mathrm{me}} + M_{33}^{\mathrm{mp}}\right)}{-M_{33}^{\mathrm{fe}} - \frac{c_{\mathrm{f}}}{c_{\mathrm{m}}}(M_{33}^{\mathrm{me}} + M_{33}^{\mathrm{mp}})} \tag{62}$$

$$B_{34}^{\mathrm{f}} = \frac{M_{34}^{\mathrm{fe}} - M_{34}^{\mathrm{me}} - M_{34}^{\mathrm{mp}}}{-M_{33}^{\mathrm{fe}} - \frac{c_{\mathrm{f}}}{c_{\mathrm{m}}}(M_{33}^{\mathrm{me}} + M_{33}^{\mathrm{mp}})} \tag{63}$$

$$B_{35}^{\mathrm{f}} = \frac{M_{35}^{\mathrm{fe}} - M_{35}^{\mathrm{me}} - M_{35}^{\mathrm{mp}}}{-M_{33}^{\mathrm{fe}} - \frac{c_{\mathrm{f}}}{c_{\mathrm{m}}}(M_{33}^{\mathrm{me}} + M_{33}^{\mathrm{mp}})} \tag{64}$$

$$B_{36}^{\mathrm{f}} = \frac{M_{36}^{\mathrm{fe}} - M_{36}^{\mathrm{me}} - M_{36}^{\mathrm{mp}}}{-M_{33}^{\mathrm{fe}} - \frac{c_{\mathrm{f}}}{c_{\mathrm{m}}}(M_{33}^{\mathrm{me}} + M_{33}^{\mathrm{mp}})} \tag{65}$$

As in the elastic matrix case, the fiber stress increment is now written in terms of a generally unknown fiber effective stress increment, and generally known external applied stress and temperature increments. The correct fiber effective stress increment balances a first order Taylor expansion of the fiber stress increment.

$$\mathrm{d}\bar{\sigma}^{\mathrm{f}} = \frac{\partial \bar{\sigma}^{\mathrm{f}}}{\partial \sigma^{\mathrm{f}}_{11}}\,\mathrm{d}\sigma^{\mathrm{f}}_{11} + \frac{\partial \bar{\sigma}^{\mathrm{f}}}{\partial \sigma^{\mathrm{f}}_{22}}\,\mathrm{d}\sigma^{\mathrm{f}}_{22} + \frac{\partial \bar{\sigma}^{\mathrm{f}}}{\partial \sigma^{\mathrm{f}}_{33}}\,\mathrm{d}\sigma^{\mathrm{f}}_{33} + \frac{\partial \bar{\sigma}^{\mathrm{f}}}{\partial \sigma^{\mathrm{f}}_{12}}\,\mathrm{d}\sigma^{\mathrm{f}}_{12} + \frac{\partial \bar{\sigma}^{\mathrm{f}}}{\partial \sigma^{\mathrm{f}}_{13}}\,\mathrm{d}\sigma^{\mathrm{f}}_{13} + \frac{\partial \bar{\sigma}^{\mathrm{f}}}{\partial \sigma^{\mathrm{f}}_{23}}\,\mathrm{d}\sigma^{\mathrm{f}}_{23} \tag{66}$$

Once the fiber effective stress increment is known, the fiber stress increment is calculated from Eq. (58), and the matrix stress increment may be directly obtained,

$$\{\mathrm{d}\sigma^{\mathrm{m}}\} = [B_{\mathrm{m}}]\{\mathrm{d}\sigma^{\mathrm{ext}}\} + \left\{0, 0, \frac{\mathrm{d}\varepsilon^{\mathrm{ft}}_{33} + \mathrm{d}T(\alpha^{\mathrm{f}} - \alpha^{\mathrm{m}})}{\frac{c_{\mathrm{m}}}{c_{\mathrm{f}}} M^{\mathrm{fe}}_{33} + M^{\mathrm{me}}_{33} + M^{\mathrm{mp}}_{33}}, 0, 0, 0\right\}^{\mathrm{T}} \tag{67}$$

where B_{m}, the matrix stress concentration tensor, is written

$$B_{\mathrm{m}} = \begin{bmatrix} 1 & 0 & 0 & 0 & 0 & 0 \\ 0 & 1 & 0 & 0 & 0 & 0 \\ B^{\mathrm{m}}_{31} & B^{\mathrm{m}}_{32} & B^{\mathrm{m}}_{33} & B^{\mathrm{m}}_{34} & B^{\mathrm{m}}_{35} & B^{\mathrm{m}}_{36} \\ 0 & 0 & 0 & 1 & 0 & 0 \\ 0 & 0 & 0 & 0 & 1 & 0 \\ 0 & 0 & 0 & 0 & 0 & 1 \end{bmatrix} \tag{68}$$

$$B^{\mathrm{m}}_{31} = \frac{M^{\mathrm{fe}}_{31} - M^{\mathrm{me}}_{31} - M^{\mathrm{mp}}_{31}}{\frac{c_{\mathrm{m}}}{c_{\mathrm{f}}} M^{\mathrm{fe}}_{33} + M^{\mathrm{me}}_{33} + M^{\mathrm{mp}}_{33}} \tag{69}$$

$$B^{\mathrm{m}}_{32} = \frac{M^{\mathrm{fe}}_{32} - M^{\mathrm{me}}_{32} - M^{\mathrm{mp}}_{32}}{\frac{c_{\mathrm{m}}}{c_{\mathrm{f}}} M^{\mathrm{fe}}_{33} + M^{\mathrm{me}}_{33} + M^{\mathrm{mp}}_{33}} \tag{70}$$

$$B^{\mathrm{m}}_{33} = \frac{\frac{1}{c_{\mathrm{f}}} M^{\mathrm{fe}}_{33}}{\frac{c_{\mathrm{m}}}{c_{\mathrm{f}}} M^{\mathrm{fe}}_{33} + M^{\mathrm{me}}_{33} + M^{\mathrm{mp}}_{33}} \tag{71}$$

$$B^{\mathrm{m}}_{34} = \frac{-M^{\mathrm{mp}}_{34}}{\frac{c_{\mathrm{m}}}{c_{\mathrm{f}}} M^{\mathrm{fe}}_{33} + M^{\mathrm{me}}_{33} + M^{\mathrm{mp}}_{33}} \tag{72}$$

$$B^{\mathrm{m}}_{35} = \frac{-M^{\mathrm{mp}}_{35}}{\frac{c_{\mathrm{m}}}{c_{\mathrm{f}}} M^{\mathrm{fe}}_{33} + M^{\mathrm{me}}_{33} + M^{\mathrm{mp}}_{33}} \tag{73}$$

$$B^{\mathrm{m}}_{36} = \frac{-M^{\mathrm{mp}}_{36}}{\frac{c_{\mathrm{m}}}{c_{\mathrm{f}}} M^{\mathrm{fe}}_{33} + M^{\mathrm{me}}_{33} + M^{\mathrm{mp}}_{33}} \tag{74}$$

The martensite fraction increment is again obtained from Eqs. (1)–(3), and the external strain increment is given by Eq. (57). The applied stress, temperature, fiber stress, fiber effective stress, matrix stress, fiber martensite fraction, fiber elastic modulus, and composite external strain are then updated in preparation for the solution of the next increment.

4. Comparisons with experiment

The theory developed in the previous section may now be used to model the thermal–mechanical behavior of NiTi shape memory alloy fiber actuated aluminum metal matrix composites. Specifically, we will use the present theory to model the self-thermal-plastic compression behavior of a prestrained composite during an unconstrained (external stress free) heating process in order to obtain comparisons between calculated results and existing experimental measurements.

4.1. Experimental materials, testing procedures and results

Armstrong and Lorentzen have recently obtained the first experimental confirmation of self-thermal-plastic behavior in a consolidated metal matrix composite (Armstrong and Lorentzen, 2000). In this study, three 50.7 at.% NiTi actuated 6082-T4 aluminum metal matrix composite specimens, and two homogeneous 6082-T4 control specimens were produced from a single hot pressing treatment. Image analysis of a composite specimen indicated a fiber volume fraction of approximately 14.5%. Each specimen was subjected to a testing procedure consisting of an initial room temperature, 5% tensile elongation–unloading process, and a subsequent room temperature to 120°C unconstrained (external stress free) heating process. During the tensile process, the applied stress was periodically reduced by approximately 20 MPa to halt straining, at which point in situ neutron diffraction measurements were made. The load reductions were made at approximately every 25 MPa during the steep portion of the tensile loading, and at approximately every 0.5% strain during stabilized plastic straining. Fig. 2(a) shows that the linear elastic response of the composite and homogeneous control materials were very similar up to approximately 30 MPa. The mechanical responses of the materials significantly differ upon further loading. The homogeneous control material exhibits a well-defined yield point at approximately 140 MPa, followed by plastic flow accompanied by high work hardening. The composite exhibits greater compliance than the homogeneous material up to the homogeneous material yield point. This feature is explained by the early initiation of plastic flow in the matrix under the effects of a tensile thermal residual stress. Continued loading of the composite material results in a steady decrease in tangent modulus up to a weakly defined upper yield point at approximately 1.35% strain. Beyond this point, the composite exhibits low work hardening relative to the

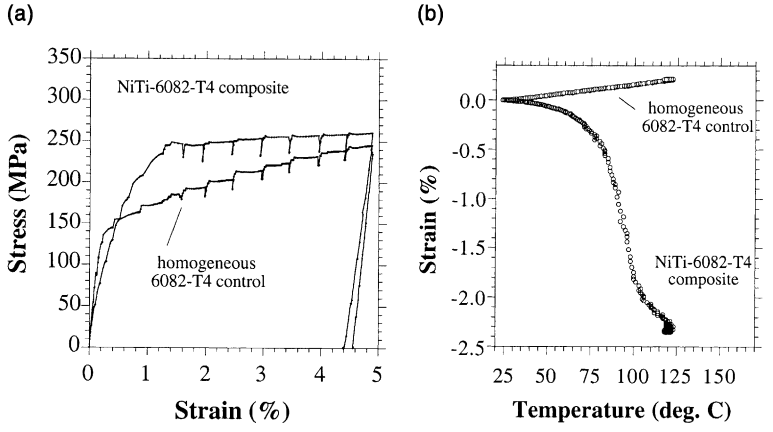

Fig. 2. Macroscopic thermal–mechanical measurements (a) room temperature tensile measurements, (b) strain as a function of temperature during the room temperature to 120°C unconstrained heating process.

homogeneous control material. Finally, the unloading modulus of the composite is significantly less than that of the homogeneous control.

Following tensile unloading, the test materials remained at room temperature for approximately 1 h before they were subjected to a 1°C/min, room temperature to 120°C unconstrained heating process. Fig. 2(b) shows that the composite exhibited a very large, nonlinear thermal contraction, while the homogeneous control exhibited the expected linear thermal expansion. The composite exhibits a negative strain versus temperature slope immediately on initiation of heating, with the strain versus temperature slope steadily increasing to a maximum value at approximately 95°C. Beyond 95°C the strain versus temperature slope decreases due to the saturation of the fiber shape memory transformation. The size of the compression strain of the composite (≈2.2%) clearly indicates that large scale matrix plastic flow was induced by a powerful shape memory response in the NiTi fiber actuators.

4.2. Input to the model

Table 1 lists input parameter values used for the modeling calculations presented in this section. The fiber volume fraction of the composite was obtained by quantitative image analysis of a test specimen central cross section. The model fiber elastic and thermal expansion properties were obtained from Dunand et al. (1996) and Jackson et al. (1972) respectively. The model NiTi fiber transformation parameters and aluminum matrix flow model parameters were selected for best fit to the experimental mechanical measurements. Fig. 3 shows that the mechanical description of the composite matrix material included in the present model adequately matches experimental measurements.

4.3. Analysis of the experiment

The present model treatment begins with the initialization of temperature, external stress, composite internal stress, and fiber phase content. In the present case, the initial temperature was measured as 20°C, and the specimen external stress was at all times equal to zero. The composite longitudinal internal stress

Table 1
Model properties

Composite geometric properties	
V_f, fiber volume fraction	14.5%
Fiber longitudinal direction	x_3
Ni–Ti fiber properties	
A_A (°C)	31.0
C_A (MPa/°C)	20.0
s_a	140
E_f (GPa)	69.0
α^f (/°C)	11.0×10^{-6}
v^f, fiber Poisson's ratio	0.33
6082-T4 Al matrix properties	
E_m (GPa)	69.5
v^m matrix Poisson's ratio	0.33
α^m (/°C)	23.4×10^{-6}
Matrix plastic flow model, $\varepsilon_p = A(\sigma - \sigma_y)^n$	
σ_y (0.2%, MPa)	156
A (MPa)	395
n	0.28

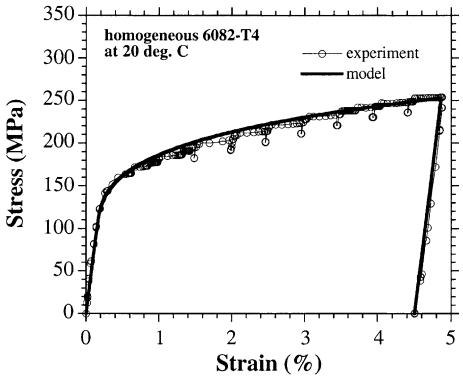

Fig. 3. Comparison between model and experimental homogeneous aluminum matrix stress–strain behavior during the low temperature prestrain process.

was measured by neutron diffraction as 220 MPa tension in the NiTi fibers and 37 MPa compression in the aluminum matrix. The remaining transverse and shear internal stress components are assumed trivial. We may identify the initial phase content of the composite fiber actuators by assuming that all of the residual strain that exists in the composite after the room temperature unloading process (shown in Fig. 2) is recoverable. Therefore, the value of the recoverable strain ε_{pl} is set equal to 4.4% while the initial martensite fraction, ξ_0, is set equal to 1.

The model calculation proceeds with discrete increases in temperature. As the temperature increases the composite fiber actuators suffer a phase transformation process which converts martensitic phase content back to the parent austenitic phase content. Fig. 4 shows the martensite fraction versus temperature behavior of the NiTi fiber actuators in the model composite during the unconstrained heating process. The fiber martensite to austenite recovery transformation is strongly shifted to higher temperatures, and spans a much larger temperature range than would be the case for stress free homogeneous NiTi. The slope of the plot significantly increases beyond ≈75°C, at which point large scale plastic flow occurs in the aluminum matrix material. Fig. 5 explains the transformation temperature shift by showing the calculated fiber von Mises equivalent stress versus temperature behavior, with a mesh overlay, the height of which is proportional to transformation intensity. The stress in the fiber strongly increases as the fiber stress–temperature

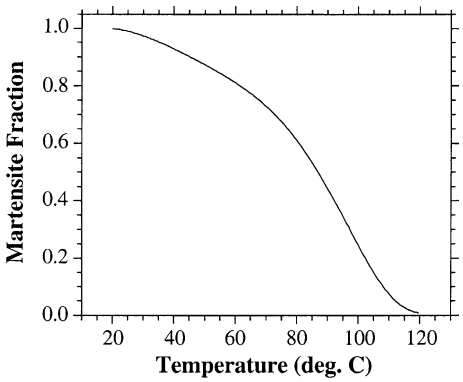

Fig. 4. Model martensite fraction versus temperature behavior during the unconstrained (external stress free) heating process. The fiber martensite to austenite recovery transformation is shifted to higher temperatures by the development of large longitudinal tensile stress in the actuating NiTi fibers.

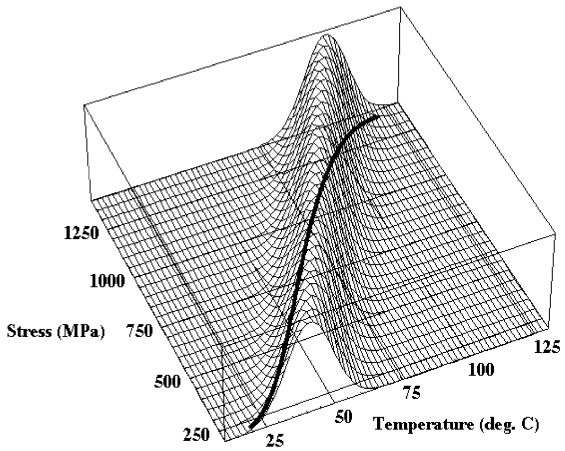

Fig. 5. Model fiber von Mises equivalent stress versus temperature behavior. The mesh height is proportional to the martensite to austenite shape recovery transformation intensity. The equivalent stress in the fiber strongly increases as the fiber stress–temperature state enters nontrivial transformation intensity due to the mechanical constraint imposed by the composite matrix.

state enters nontrivial transformation intensity due to the mechanical constraint imposed by the composite matrix. The increase in fiber equivalent stress in turn necessitates strong increases in temperature before further phase transformation may occur.

Fig. 6 compares the calculated and measured thermal strain versus temperature behavior of the composite. As the temperature increases, the fiber stress–temperature state enters increasing phase transformation intensity, resulting in strong increases in fiber longitudinal tensile stress, matrix longitudinal compressive stress and composite compressive longitudinal external strain. Sufficient temperature brings the matrix stress state to the point of plastic yield. The composite then exhibits a very unusual, large nonlinear self-thermal-plastic compression response.

Fig. 6 shows that at low and moderate temperatures the quantitative agreement between measured and calculated results is good, however clear attenuation of the fiber shape memory response is indicated at

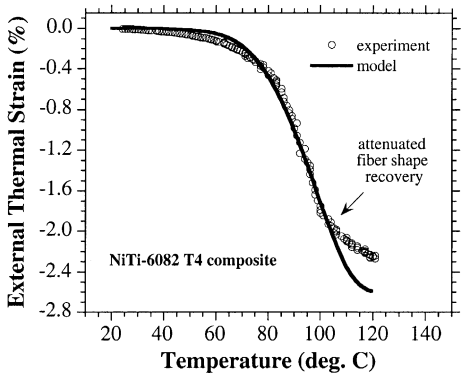

Fig. 6. Comparison between model and experimental composite external thermal strain versus temperature behavior. The composite external thermal strain temperature gradient increases as the composite aluminum metal matrix suffers plastic yielding. The sharp disagreement between model and experiment at temperatures above ≈100°C clearly indicates a significant attenuation of the fiber shape memory response.

temperatures above 100°C. The observed attenuation in the intensity of shape recovery in the experimental composite may result from the tensile plastic failure of the NiTi actuating fibers as indicated in an earlier experiment (Armstrong, et al., 1998), or from the development of a significant amount of unrecoverable strain in the composite actuators during deformation processes.

5. Summary and conclusions

The present work develops a quantitative theory of the self-thermal-plastic response of NiTi shape memory alloy actuated metal matrix composite materials. Model calculations are compared with existing experimental data obtained from a testing procedure consisting of an initial room temperature, 5% tensile elongation process, and a subsequent room temperature to 120°C unconstrained (external stress free) heating process. This effort supports the following conclusions:

(1) We may construct a general multiaxial description of the phase transformations of NiTi shape memory alloys by establishing distributed, J_2 invariant transformation yield functions and an associated transformation flow rule. The distributed transformation yield functions associate a transformation intensity to each ten dimensional stress–temperature coordinate. The shape memory alloy phase state varies as the stress–temperature state translates along stress–temperature trajectories which result in forward penetrations of nontrivial transformation intensity contours.

(2) Consider a specific thermal–mechanical testing procedure consisting of an initial low temperature tensile elongation process, and a subsequent unconstrained (external stress free) heating process. During the unconstrained heating process the composite fiber actuators attempt to recover pseudo-plastic strain imparted during the room temperature tensile prestrain process. As the temperature increases, the fiber stress–temperature state enters increasing phase transformation intensity, resulting in strong increases in fiber longitudinal tensile stress, matrix longitudinal compressive stress and composite compressive longitudinal external strain. Sufficient temperature brings the matrix stress state to the point of plastic yield. The composite then exhibits a very unusual, large nonlinear self-thermal-plastic compression response, recovering approximately 2.2% strain.

(3) At low and moderate temperatures the quantitative agreement between measured and calculated results is good, however clear attenuation of the fiber shape memory response is indicated at temperatures above 100°C. The observed attenuation in the intensity of shape recovery in the experimental composite may result from the tensile plastic failure of the NiTi actuating fibers as indicated in an earlier experiment (Armstrong et al., 1998), or from the development of a significant amount of unrecoverable strain in the composite actuators during deformation processes.

Acknowledgements

The author acknowledges the support of the National Science Foundation under NSF Grant CMS-9972055, Program Officer Ken Chong.

References

Aboudi, J., 1997. The response of shape memory alloy composites. Smart Mater. Struct. 6, 1–9.

Armstrong, W.D., 1996. A one dimensional model of a shape memory alloy fiber reinforced aluminum metal matrix composite. J. Intell. Mater. Syst. Struct. 7, 448–454.

Armstrong, W.D., Kino, H., 1995. Martensitic transformations in a NiTi fiber reinforced 6061 aluminum matrix composite. J. Intell. Mater. Syst. Struct. 6, 809–816.

Armstrong, W.D., Lorentzen, T., 1997. Fiber phase transformation and matrix plastic flow in a room temperature tensile strained NiTi shape memory alloy fiber reinforced 6082 aluminum matrix composite. Scripta Materialia 36, 1037–1043.

Armstrong, W.D., Lorentzen, T., 2000. Large self-thermal-plastic deformation in a NiTi shape memory alloy fiber actuated aluminum metal matrix composite, Acta Materialia, submitted for publication.

Armstrong, W.D., Lorentzen, T., et al., 1998. An experimental and modeling investigation of the external strain, internal stress and fiber phase transformation behavior of a NiTi actuated aluminum metal matrix composite. Acta Materialia 46, 3455–3466.

Bo, Z.H., Lagoudas, D.C., 1999. Thermomechanical modeling of polycrystalline SMA under cyclic loading, part II: material characterization and experimental results for a stable transformation cycle. Int. J. Engng. Sci. 37, 1141–1173.

Boyd, J.C., Lagoudas, D.C., 1994. Thermomechanical response of shape memory alloy composites. J. Intell. Mater. Syst. Struct. 5, 333–346.

Brinson, L.C., 1993. One-dimensional constitutive behavior of shape memory alloys: thermomechanical derivation with non-constant material functions and redefined martensite internal variable. J. Intell. Mater. Syst. Struct. 4, 229–242.

Brinson, L.C., Huang, M.S., 1996. Simplifications and comparisons of shape memory alloy constitutive models. J. Intell. Mater. Syst. Struct. 7, 108–114.

Dautovich, D.P., Purdy, G.R., 1965. Phase transformations in TiNi. Canadian Metallurg. Quart. 4, 129–143.

de Lange, R.G., Ziderveld, J.A., 1968. Shape-memory effect and the martensitic transformation of TiNi. J. Appl. Phys. 39, 2195–2200.

Dunand, D.C., Mari, D., et al., 1996. NiTi and NiTi–TiC composites: part IV. Neutron diffraction study of twinning and shape-memory recovery. Metallurg. Mater. Trans. A 27A, 2820–2836.

Dvorak, G.J., Bahei-El-Din, Y.A., 1982. Plasticity analysis of fibrous composites. J. Appl. Mech. 49, 327–335.

Furuya, Y., Sasaki, A., et al., 1993. Enhanced mechanical properties of TiNi shape memory fiber/Al matrix composite. Mater. Trans. JIM 34, 224–227.

Hamada, K., Lee, J.H., et al., 1998. Thermomechanical behavior of TiNi shape memory alloy fiber reinforced aluminum matrix composite. Metallurg. Trans. 29A, 1127–1135.

Jackson, C., Wagner, H., et al., 1972. 55 Nitinol - the alloy with a memory: its physical metallurgy, properties and applications. NASA-SP 5110.

Knowles, K.M., Smith, D.A., 1981. The crystallography of the martensitic transformation in equiatomic nickel–titanium. Acta Metallurgica 29, 101–110.

Liang, C., Rogers, C.A., 1990. One-dimensional thermomechanical constitutive relations for shape memory materials. J. Intell. Mater. Syst. Struct. 1, 207–234.

Ling, H.C., Kaplow, R., 1980. Phase transitions and shape memory in NiTi. Metallurg. Trans. A 11A, 77–83.

Michal, G.M., Sinclair, R., 1981. The structure of TiNi martensite. Acta Cryst. B 37, 1803–1807.

Miyazaki, S., Otsuka, K., 1986. Deformation and transition behavior associated with the R-phase in Ti–Ni alloys. Metallurg. Trans. A 17A, 53–63.

Otsuka, K., Shimizu, K., 1986. Pseudoelasticity and shape memory effects in alloys. Int. Metal Rev. 31, 93–114.

Shaw, J.A., Kyriakides, S., 1995. Thermomechanical aspects of NiTi. J. Mech. Phys. Solids 43, 1243–1281.

Tanaka, K., Nagaki, S., 1982. A thermomechanical description of materials with internal variables in the process of phase transformation. Ingenieur-Archiv 51, 287–299.

Taya, M., Furuya, Y., et al., 1993. Strengthening mechanisms of TiNi shape memory fiber/Al matrix composite. Proc. Smart Materials, SPIE.

Wayman, C.M., 1981. The shape memory effect. Metals Forum 4 (3), 135–141.

Wei, Z.G., Sandstrom, R., et al., 1998. Shape memory materials and hybrid composites for smart systems – part II shape memory hybrid composites. J. Mater. Sci. 33, 3763–3783.

Ziegler, H., 1959. A modification of Prager's hardening rule. Quart. Appl. Math. 17, 55–65.